HHS Public Access

Author manuscript

Nat Neurosci. Author manuscript; available in PMC 2014 March 01.

Published in final edited form as:

Nat Neurosci. 2013 September ; 16(9): 1324–1330. doi:10.1038/nn.3494.

Linear Transformation of Thalamocortical input by Intracortical Excitation

Ya-tang Li[1,4], **Leena A. Ibrahim**[1,4], **Bao-hua Liu**[1,4], **Li I. Zhang**[1,3], and **Huizhong Whit Tao**[1,2,*]

[1]Zilkha Neurogenetic Institute, University of Southern California, Los Angeles, CA 90089, USA

[2]Department of Cell and Neurobiology, University of Southern California, Los Angeles, CA 90089, USA

[3]Department of Physiology and Biophysics, University of Southern California, Los Angeles, CA 90089, USA

[4]Graduate Programs, Keck School of Medicine, University of Southern California, Los Angeles, CA 90089, USA

Abstract

Neurons in thalamorecipient layers of sensory cortices integrate thalamocortical and intracortical inputs. Although their functional properties can be inherited from the convergence of thalamic inputs, the roles of intracortical circuits in thalamocortical transformation of sensory information remain unclear. Here, by reversibly silencing intracortical excitatory circuits with optogenetic activation of parvalbumin-positive inhibitory neurons in mouse primary visual cortex, we compared visually-evoked thalamocortical input with total excitation in the same layer 4 pyramidal neurons. We found that intracortical excitatory circuits preserve the orientation and direction tuning of thalamocortical excitation, with a linear amplification of thalamocortical signals by about threefold. The spatial receptive field of thalamocortical input is slightly elongated, and is expanded by intracortical excitation in an approximately proportional manner. Thus, intracortical excitatory circuits faithfully reinforce the representation of thalamocortical information, and may influence the size of the receptive field by recruiting additional inputs.

Introduction

Neurons in layer 4 of the primary visual cortex (V1) receive excitatory inputs from two major sources: the feedforward thalamocortical input and the intracortical input from other cortical neurons[1,2]. Since the proposal that a linear spatial arrangement of thalamic neuron receptive fields results in orientation-tuned input to simple cells was first made[3–5], the respective roles of thalamocortical and intracortical inputs in generating cortical orientation selectivity have been intensively studied[6]. In one view, the feedforward input is sufficient for generating sharp orientation selectivity[7,8]. In a second view, the feedforward input only provides a weak orientation bias, and orientation selectivity is greatly strengthened by

*Correspondence should be addressed to: H.W.Tao, htao@usc.edu.

excitation (e.g. recurrent excitation) from other cortical neurons tuned to the same orientation[9–14].

Previously, several experimental methods have been used to silence cortical spikes and isolate thalamocortical input: 1) pharmacological silencing of the cortex by activating $GABA_A$ receptors with muscimol[15,16]; 2) cooling of the cortex[7]; 3) electrical shocks in the cortex to produce an inhibitory widow of hundreds of milliseconds during which spikes cannot be generated[8]. Results from these previous studies in general agree with the notion that neurons in layer 4 inherit their functional properties from the relay of thalamic inputs. However, due to the technical limitations in previous methods, e.g. the non-specific effects on synaptic transmission[17,18] or difficulties of reversible applications[15], the precise contributions of thalamocortical and in particular intracortical circuits to cortical orientation selectivity and other functional properties remain to be determined. Optogenetic approaches[19,20] provide an unprecedented advantage in addressing this question, since specific activation of parvalbumin-positive (PV) inhibitory neurons alone can effectively and reversibly silence spiking of cortical excitatory neurons[21]. In this study, we combined *in vivo* whole-cell voltage-clamp recordings with optical activation of PV inhibitory neurons to isolate thalamocortical excitation from the total excitation in the same neuron. Our results indicated that intracortical excitatory circuits preserved the orientation and direction tuning of feedforward input by linearly amplifying its signals, and expanded the spatial visual receptive field by recruiting more distant inputs possibly via horizontal circuits.

Results

Optogenetic silencing of visual cortical circuits

For optogenetic silencing, we utilized the Cre/*loxP* recombination to express channelrhodopsin-2 (ChR2) in PV inhibitory neurons (see **Methods**). We injected an adeno-associated viral vector AAV2/9-EF1α-DIO-ChR2-EYFP into the V1 of PV-Cre tdTomato mice. As shown by the EYFP fluorescence in cortical slices from animals two weeks after the injection, ChR2 was expressed across cortical layers (Fig. 1a, top) and specifically in PV neurons (Fig. 1a, bottom). We applied illumination of the exposed visual cortical surface with blue LED light (470 nm) via an optical fiber. In the V1 region expressing EYFP, we carried out *in vivo* cell-attached recordings from excitatory neurons to examine the effects of optical activation of PV neurons. We found that LED illumination resulted in complete silencing of visually evoked spikes shortly after its onset, and that the effect sustained throughout the duration of the illumination (Fig. 1b, left). We observed such silencing effect throughout layer 4–6 (Fig. 1b, right). To confirm that the silencing effect was through activating PV inhibitory neurons, we carried out visually guided recordings from PV neurons under two-photon imaging[22,23] (see **Methods**). We found that opposite to the effect on excitatory neurons, LED illumination dramatically increased the firing rate of PV neurons (Fig. 1c). After an initial reduction, the high firing rate could be maintained throughout the duration of LED illumination which lasted for a few seconds (Fig. 1c, left). Furthermore, whole-cell voltage-clamp recordings from excitatory neurons revealed that LED illumination alone induced a large sustained current, the reversal potential of which was consistent with that of Cl^- currents (Fig. 1d). These experiments demonstrated that

optogenetic activation of PV inhibitory neurons effectively silenced spiking of cortical excitatory neurons and thus eliminated intracortical connections.

Previous studies in auditory and visual cortices have suggested that thalamocortical axon terminals contain $GABA_B$ receptors[17,18]. Activation of these presynaptic receptors by GABA agonists such as muscimol can reduce transmitter release[15,16]. We thus examined whether optogenetic activation of PV neurons could potentially lead to a reduction of thalamocortical transmission caused by a spillover of GABA released from inhibitory synapses made by PV cells. We recorded extracellular ensemble currents evoked by flash noise stimuli in layer 4 (see **Methods**), which reflect the summed neuronal and synaptic activity within a local cortical area[24]. We then delivered LED light immediately before the visual stimulus. If there is a reduction of presynaptic release, we would expect to see a decrease in the visually evoked ensemble current. This effect is also expected to last for 1–2 seconds since the decay time constant for $GABA_B$ receptors is 2.8 s[25]. We found that LED illumination directly induced a negative ensemble current **(**Fig. 1e, top). Nevertheless, the amplitude of the following visually evoked current was not apparently reduced (Fig. 1e, bottom), neither was its temporal profile altered (Fig. 1e, top). Additionally, we examined visually evoked excitatory currents in layer 4 neurons, applying similar visual stimulation without and with coupling LED illumination (Fig. 1f, top). Again, we did not observe a reduction of the visually evoked excitatory currents in individual cortical cells (Fig. 1f, bottom). Altogether, these control experiments suggested that there was no presynaptic inhibition caused by LED-induced GABA release, possibly because GABAergic synapses made by PV neurons are relatively distant from thalamocortical synapses. Thus, the optogenetic activation of PV neurons could be an effective method to silence the cortex without significantly affecting thalamocortical transmission.

Scaling of orientation-tuned thalamocortical input

We next examined excitatory synaptic responses to single drifting bars at 12 different directions without and with coupling LED illumination. We carried out *in vivo* whole-cell voltage-clamp recordings with a Cs^+-based internal solution from layer 4 excitatory neurons (Supplementary Fig. 1a) and clamped the cells at the reversal potential for inhibitory currents, which was determined from LED-evoked currents (see Fig. 1d). We interleaved control trials with visual stimulus only and trials with PV neuron photostimulated. As shown in an example cell, LED illumination reduced the amplitude of excitatory currents to all directions of bar movement (Fig. 2a, left). In addition to the change in amplitude, we observed that the response onset latencies were prolonged (Fig. 2a, left, dotted curves). To quantify orientation tuning, we measured peak current amplitudes after smoothing the current traces with a 40 ms sliding window for averaging. Despite the general reduction in amplitude after cortical silencing, there was little change in orientation tuning of excitatory input, as shown by the normalized tuning curves (Fig. 2a, right). This result suggested that the excitatory responses were reduced by a similar fraction across orientations. In another word, tuning curve was scaled down. We quantified the scaling factor from the slope of linear fitting of response amplitudes in LED on versus control trials (Fig. 2a, right, bottom). As shown by the example cell, the data were well fitted by a linear relationship, and the scaling factor was well below 1 (Fig. 2a, right, bottom). We showed polar graph plots of

orientation tuning of excitatory currents for more example cells (Fig. 2b). In general, tuning shapes looked similar without and with LED illumination, with response amplitudes clearly reduced.

We averaged the normalized excitatory tuning curves of all the recorded cells (19 from 19 mice). This "population" tuning curve was largely unchanged after cortical silencing (Fig. 2c), supporting the notion of scaling. It is worth noting that the isolated thalamocortical input (as well as the total excitatory input) was weakly tuned, with only a small difference between the responses to the preferred and orthogonal orientations (Fig. 2c). To examine the change of tuning for each individual cell, we calculated a global orientation selectivity (gOSI, equivalent to 1 – circular variance, see **Methods**). We found that orientation tuning of excitatory input was not significantly changed ($P > 0.05$, bootstrap analysis) after cortical silencing in all individual cells except two (Fig. 2d). Neither was the preferred orientation changed in individual cells (Fig. 2e). The slope of linear regression (i.e. scaling factor) ranged from 0.19 to 0.71, with the mean of 0.38 (Fig. 2f). This indicated that thalamocortical input was about one third of the total excitatory input. In another word, there was a threefold amplification of thalamocortical signals by intracortical excitatory circuits. Measurements of integrated charge of synaptic currents also supported the notion that the tuning sharpness as well as the preferred orientation was preserved after silencing the cortex (Supplementary Fig. 2a, b), although the tuning of integrated charge was weaker than that measured with peak amplitude ($P = 0.018$, one-tailed paired *t*-test, $n = 19$ cells from 19 mice, comparison was made for responses in control trials).

Under our current recording conditions, the linear I–V relationship and the proximity of the derived reversal potential of LED-evoked currents to the expected reversal potential of inhibitory currents (Fig. 1d) suggested that the somatic voltage clamp was adequate. Therefore synaptic inputs relatively close to the soma might be reasonably well clamped. The thalamocortical input to layer 4 neurons, synapses of which are located proximal to the soma, is expected to be better clamped and less affected by space-clamp errors and cable attenuation compared to inputs onto distal dendrites (also see the discussion in **Methods**). Nevertheless, we recognize that there are potential deviations of measured synaptic amplitude from the bona fide amplitude caused by space-clamp errors and cable attenuation, which need to be investigated in the future.

Intracortical excitation preserves direction tuning

Layer 4 neurons exhibit not only orientation selectivity, but also direction selectivity[22,26]. In order to understand the relationship between direction selectivity of spike response and that of excitatory input, we carried out sequential cell-attached and whole-cell recordings (with a K^+-based internal solution) from the same neurons in wild type mice (see **Methods**). The spikes recorded in the cell-attached mode allowed us to quantify the direction selectivity of the cell's output response, and the subsequent whole-cell recording allowed us to examine the underlying excitatory drive. As shown by an example cell (Fig. 3a, b), although the cell exhibited clearly direction-selective spike responses, the amplitude of excitatory current only showed a slight difference between the preferred and null directions. Thus, consistent with what has been previously reported, the spike threshold greatly amplified the selectivity

of output response[27]. The plot of direction selectivity index (DSI) of spike response versus that of excitatory current revealed a strong linear relationship (Fig. 3c). In addition, the preferred direction of spike response was essentially the same as that of excitatory drive (Fig. 3d). These results indicated that the selectivity of spike response strongly correlated with that of excitatory input, which might be employed to predict direction selectivity of the neurons.

We next examined how direction tuning of excitatory drive is determine d by thalamocortical and intracortical inputs. We found that the direction tuning of excitatory drive was not changed by silencing intracortical inputs, as shown by the superimposed average direction tuning curves without and with LED illumination (Fig. 3e). On an individual cell basis, DSI of thalamocortical excitation was also similar to that of total excitation (Fig. 3f), and the preferred direction was unchanged after silencing the cortex (Fig. 3g). Similar conclusions could be made when the integrated charge of excitatory current was considered (Supplementary Fig. 2c, d). Together these results further demonstrated a linear amplification effect of intracortical excitatory circuits. The feedforward input to layer 4 neurons was already direction-tuned, and the intracortical excitation increased the gain of the signal, without affecting its tuning property.

Intracortical excitation expands visual receptive field

Taking advantage of drifting-bar evoked responses, we were able to estimate the shape and size of the spatial receptive field of excitatory drive. We estimated the receptive field boundary based on the moving bar speed and the response latency at each stimulus direction (Fig. 4a, top left). We found that the response onset latency was prolonged in the presence of LED illumination at all stimulus directions (Fig. 4a, bottom and Supplementary Fig. 3a), suggesting that the visual receptive field had “shrunk” after cortical silencing. We derived receptive field outlines for the total excitation and thalamocortical excitation respectively (see **Methods**) (Fig. 4a, bottom), and fitted it to an ellipse (Fig. 4a, top right). We found that the derived receptive fields were both slightly elongated, and the major axes of both receptive fields (i.e. the axis for receptive field elongation) were similar as the preferred orientation of the cell’s excitatory drive under moving stimuli (marked by the blue arrows in Fig. 4a). The observation in this example cell suggested that the size of spatial receptive field was reduced in the presence of LED illumination, while its overall shape was not changed apparently.

In a total of 19 recorded cells, we observed that the onset latency of excitatory responses to moving bars (averaged for two opposite directions) increased more for the preferred than the orthogonal orientation (Supplementary Fig. 3b), suggesting more receptive field shrinkage along the preferred orientation. As a control, the onset of responses to flash stimuli was not changed in the presence of LED illumination (Fig. 4b), indicating that the subcortical conduction of visual signals was not affected by the cortical silencing. From the response onset latencies, the estimated receptive field size (defined as the long axis of the fitted ellipse) for total excitatory input was 45.6 ± 11.7° (mean ± s.d.). The estimated receptive field was reduced to 32.4 ± 10.2° after cortical silencing (P = 5.16e–10, two-tailed paired t-test, n = 19 cells from 19 mice, Fig. 4c). Despite the reduction in size, the receptive field

shape remained roughly the same, as reflected by the largely unchanged angle of the major receptive field axis ($P = 0.52$, two-tailed paired *t*-test, Fig. 4d) and the unchanged aspect ratio ($P = 0.22$, two-tailed paired *t*-test, Fig. 4e), which was defined as the ratio of the length of major versus minor receptive field axis[5,28]. In addition, the major axis of the estimated thalamocortical receptive field had a similar angle as the preferred orientation of the isolated thalamocortical response (Fig. 4f). All thalamocortical receptive fields were slightly elongated, as reflected by the aspect ratios larger than 1 but mostly smaller than 2, with a mean of 1.63 (Fig. 4e). Furthermore, there was a strong linear correlation between the orientation selectivity level of thalamocortical responses and the aspect ratio of the estimated thalamocortical receptive field (Fig. 4g).

To further confirm the receptive field shrinkage after cortical silencing, we applied conventional flash sparse stimuli to directly map the spatial receptive field (see **Methods**). We found that the receptive field indeed appeared smaller in the presence of LED illumination, as shown by an example cell (Fig. 4h). Summary results of 14 cells recorded from 14 mice showed that receptive field size was significantly decreased by eliminating intracortical excitatory inputs (from 38.2 ± 9.0° to 31.8 ± 8.6°, $P = 1.92e{-}6$, one-tailed paired *t*-test, Fig. 4i), whereas the angle of receptive field major axis and the aspect ratio were unaltered ($P = 0.4$, Fig. 4j; $P = 0.46$, Fig. 4k; two-tailed paired *t*-test). Notably, in normal conditions, the receptive field size measured with sparse flash stimuli was smaller than that estimated from drifting-bar responses ($P = 0.02$, one-tailed *t*-test), while they were not different in cortical silencing conditions ($P = 0.87$, two-tailed *t*-test). Therefore the receptive field size derived from drifting-bar responses reduced more (29.4% ± 9.8%) after cortical silencing, compared to that measured with flash stimuli (16.9% ± 8.5%, $P = 2.3e{-}4$, one-tailed *t*-test). One possible explanation was that some cortical neurons providing distant intracortical inputs were sensitive to moving stimuli, but could not be activated by sparse flash stimuli. Altogether, these results suggested that the spatial organization of thalamic inputs (i.e. the elongated arrangement) provided a basis for the orientation tuning of thalamocortical responses, and that intracortical excitatory circuits expanded the visual receptive field approximately proportionally in spatial extent.

Tuning of dLGN neurons is unaffected

Previous studies indicate that layer 6 neurons in sensory cortices project back to the thalamus and may modulate thalamic neuron activity[21,29]. To investigate the effect of silencing the cortical feedback projection on thalamic activity, we carried out cell-attached recordings in the dorsal lateral geniculate nucleus (dLGN). We found that neurons in the dLGN already exhibited moderate orientation tuning as measured either by drifting bars (Fig. 5a–c) or by drifting sinusoidal gratings (Supplementary Fig. 4a–c), consistent with a recent report[30]. Their tuning was not significantly affected by cortical silencing (Fig. 5a–c and Supplementary Fig. 4a–c), the effectiveness of which was verified in each experiment by recording in layer 6. The evoked firing rates of dLGN neurons averaged for twelve directions were unaltered after silencing the cortex (Fig. 5d and Supplementary Fig. 4d), indicating that the reduction of excitatory drive in cortical neurons could be attributed primarily to the elimination of intracortical inputs. The tuning strength of dLGN neuron

responses was slightly stronger than that of thalamocortical input, but was much weaker than that of cortical neuron spikes (Fig. 5e).

In contrast to dLGN neurons, the evoked firing rate of thalamic reticular nucleus (TRN) neurons was markedly reduced after silencing the cortex (Fig. 5f, g). These neurons essentially had no orientation tuning (Fig. 5h). Their average OSI was 0.044 ± 0.025 (mean ± s.d., n = 20 cells from 16 mice), significantly lower than that of dLGN neurons (P = 0.0018, one tailed t-test). That the firing rate of dLGN neurons was unchanged after silencing the cortex was likely due to a concurrent decrease of excitatory drive from layer 6 and inhibitory drive from the TRN[21,29], which also receives direct excitation from layer 6 of the cortex[21,29].

Discussion

As a fundamental computational property, orientation selectivity is thought to emerge in the visual cortex. Whether its generation in the thalamorecipient neurons can be solely attributed to the spatial arrangement of feedforward thalamic inputs or intracortical circuits (in particular the local recurrent network) play an indispensible role has been widely discussed[6]. In this study, by silencing intracortical excitatory connections with an optogenetic method, we showed that the feedforward input to mouse layer 4 excitatory neurons was weakly orientation-tuned. Intracortical excitation scaled up or linearly amplified the thalamocortical signals approximately threefold without modifying the input tuning property. Similarly, the direction tuning provided by thalamocortical input was unaffected through such signal amplification. In addition, our study revealed that intracortical excitatory circuits enlarged the visual receptive field without significantly modifying the receptive field shape.

The linear amplification of thalamocortical responses suggests that the feedforward input, although only weakly tuned, provides an orientation bias for driving orientation selectivity in the cortex. The tuning of thalamocortical input can be contributed by several mechanisms. First, the thalamocortical receptive field was slightly elongated, and the axis of elongation was the same as the preferred orientation of thalamocortical responses to drifting bars. These results are in line with the original feedforward model that the spatial organization of thalamic inputs provides a fundamental basis for orientation tuning[3]. Because of the elongated spatial arrangement of thalamic inputs, a bar of preferred orientation can activate thalamic inputs more synchronously than a bar of orthogonal orientation. More synchronous inputs can generate a larger peak current, and can be more efficient in driving spiking of layer 4 cells[31]. Second, dLGN neurons themselves were orientation tuned. The convergence of LGN inputs with similar orientation preference might be sufficient for providing orientation-tuned input to a cortical neuron. However, without understanding the relationship between orientation preferences of LGN neurons and their cortical targets, the contribution of tuning of individual LGN neurons remains unclear. Furthermore, the segregation of On and Off thalamic inputs[6,32], which has not been examined in the current study, may also contribute to the orientation tuning of the summed thalamocortical input.

Previous studies in cat visual cortex have been focused on membrane potential responses[7,8], which reflect a result of interplay between excitatory and inhibitory inputs. The combining

of optogenetic silencing with voltage-clamp recordings allows the direct elucidation of different excitatory components and determination of their respective contribution to cortical functional properties. Similar as in the cat visual cortex, we did not find evidence that intracortical excitatory circuits significantly sharpen orientation tuning, which had been predicted by previous theoretical models based on recurrent circuits[9–11]. Instead, excitatory responses were scaled up by a similar factor across different orientations. Such scaling or gain modulation of feedforward thalamocortical signals determined that the total excitation remained weakly tuned. The orientation selectivity of spike responses of cortical neurons was much stronger than their thalamic inputs (Fig. 5e). The sharp selectivity of output response may be eventually achieved through the effects of more broadly tuned inhibition[22,33–39] as well as of spike threshold[27,35,40–42]. In addition, non-linear mechanisms not revealed by the voltage-clamp recordings, e.g. NMDA receptor activation[43], may also serve to sharpen the tuning of output response.

What kind of intracortical circuits might be responsible for the multiplication of thalamocortical signals? Neurons with different orientation preference in the mouse visual cortex are organized in a random, “salt-and-pepper” pattern[34,44]. However, the connection probability between excitatory neurons with a similar preferred orientation is slightly higher than that between neurons preferring different orientations[34]. Such biased connectivity between cortical excitatory neurons is likely sufficient for generating the weakly tuned intracortical excitation, which is also co-tuned with the feedforward excitation. The cortical gain is roughly 2, tripling the amplitude of feedforward input. The gain modulation of excitatory drive by intracortical circuits ensures that feedforward signals are reliably and faithfully represented in the cortex.

On the other hand, intracortical circuits may provide opportunities for integrating novel information by expanding the visual receptive field. It has been thought that horizontal or lateral interactions contribute to the “silent” extra-classical receptive field, activation of which provides contextual information that can modulate responses to stimulation of the central classical receptive field of the cell[45–47]. Here we provided direct evidence that visual receptive field peripheries might be attributed to intracortical circuits. Notably, the recruitment of more distant inputs through intracortical circuits largely preserved the elongated shape of the receptive field, suggesting that the spatial integration of intracortical inputs had a bias along the preferred orientation of the cell. That is, there might be more inputs arranged along the preferred orientation than the orthogonal, contributing to the tuning of intracortical excitation[48]. Such connectivity pattern may arise during development under the guidance of correlation-based Hebbian plasticity rules[49,50]. The coherent organization of thalamocortical and intracortical inputs allows cortical neurons to faithfully reinforce the representation of thalamocortical information.

Methods

All experimental procedures used in this study were approved by the Animal Care and Use Committee of USC.

Viral injection

Female mice (45–60 days) used in experiments were generated by crossing PV-Cre mice with tdTomato reporter mice (The Jackson Laboratory, C57BL/6J background). We anaesthetized mice with 2% isoflurane, thinned the skull over V1 and performed ∼0.2 mm^2 craniotomy. We delivered the virus using a bevelled glass micropipette (tip diameter 40 – 50 μm) attached to a microsyringe pump (World Precision Instruments). Adeno-associated viruses (AAVs) to deliver ChR2 were acquired from the UPenn Viral Vector Core: AAV2/9.EF1α.DIO.hChR2(H134R)-EYFP.WPRE.hGH (Addgene 20298). We injected virus at a volume of 50 nl/injection and at a rate of 20 nl/min We performed the injection at two locations ([0.8, 2.3], [0.8, 3] mm anterior and lateral to lambda) and two depths (300 μm and 600 μm). We then sutured the scalp, and administered an analgesic (0.1 mg/kg Buprenex) to help the recovery from anaesthesia. We made *in vivo* recordings 2–3 weeks after viral injections. We examined the expression pattern of hChR2(H134R)-EYFP in each injected mouse before the experiment, and carried out recordings only in animals with a correct location of EYFP expression (1 out of 20 mice was excluded). That is, for the major experiments, there was only one animal group. In more than 300 EYFP-expressing neurons examined in 5 mice, all of them expressed tdTomato, indicating that they were all PV-positive inhibitory neurons.

Animal surgery

We sedated the mouse with EYFP expression with an intramuscular injection of chlorprothixene hydrochloride (10 mg/kg in 4 mg/ml water solution) and then anesthetized it with urethane (1.2 g/kg, i.p., at 20% w/v in saline), as previously described[23,26]. We maintained the animal's body temperature at ∼37.5° by a heating pad (Havard Apparatus, MA). We performed tracheotomy, and inserted a small glass capillary tube to maintain a free airway. We performed cerebrospinal fluid draining, removed the skull and dura mater (∼ 1 × 1 mm) over the V1, and applied artificial cerebrospinal fluid solution (ACSF, containing [in mM] 140 NaCl, 2.5 KCl, 2.5 $CaCl_2$, 1.3 $MgSO_4$, 1.0 NaH_2PO4, 20 HEPES, 11 glucose, pH 7.4) to the exposed cortical surface when necessary. We trimmed eyelashes contralateral to the recording side, and covered the eyes with ophthalmic lubricant ointment until recording, at which time we rinsed the eyes with saline and applied a thin layer of silicone oil (30,000 centistokes) to prevent drying while allowing clear optical transmission. Eye movements and the receptive field drift were negligible within the time window of our recordings[40].

In vivo electrophysiology

We pre-penetrated the pia with a broken pipette under visual guidance before *in vivo* recordings, and then performed whole-cell voltage-clamp recordings with an Axopatch 200B (Molecular Devices). The patch pipette had a tip opening of ∼2 μm (4 – 5 MΩ impedance). The Cs^+-based intrapipette solution used for voltage-clamp recordings contained (in mM): 125 Cs-gluconate, 5 TEA-Cl, 4 MgATP, 0.3 GTP, 8 disodium phosphocreatine, 10 HEPES, 10 EGTA, 2 CsCl, 1 QX-314, 0.75 MK-801, biocytin 1%, pH 7.25. The K^+-based intrapipette solution used for sequential cell-attached and whole-cell recordings contained (in mM): 130 K-gluconate, 4 MgATP, 0.3 GTP, 8 disodium

phosphocreatine, 10 HEPES, 10 EGTA, 2 KCl, biocytin 1%, pH 7.25. The pipette capacitance and whole-cell capacitance were compensated completely, and series resistance was compensated by 50% – 60% (at 100 μs lag). A −11 mV junction potential was corrected. Signals were filtered at 2 kHz and sampled at 10 kHz. We isolated excitatory currents by clamping the cell at the reversal potential for LED-evoked Cl^- currents (−64 ± 6 mV), which was determined for each individual experiment. As discussed previously[36,40], our whole-cell recording method with relatively large pipettes highly biases sampling towards pyramidal neurons. For cell-attached recordings only, the pipette contained ACSF, and we recorded spikes in the voltage-clamp mode, with a small commend potential applied to achieve a zero baseline current. The spike signal was filtered at 10 kHz and sampled at 20 kHz. The spike waveform of recorded excitatory neurons had a trough-to-peak interval of 0.85 ± 0.10 ms (n = 35 cells). We recorded the extracellular ensemble currents with a patch pipette filled with 1M NaCl, under voltage clamp with a holding voltage of 0 mV. Signals were filtered at 10 kHz and sampled at 20 kHz.

We determined the depth location of layer 4 (370 μm to 510 μm from the pia) based on the expression pattern in a layer-4-specific Cre line (Scnn1a-Tg3-Cre, the Jackson laboratory) crossed with the tdTomato reporter line (see Supplementary Fig. 1a). The layer assignment of the blindly recorded neurons was made mostly according to the vertical travel distance of the electrode. The assignment was reasonably precise because our use of a high-magnification objective (40×) on the microscope allowed a precise identification of the cortical surface and our application of pre-penetration minimized the dimpling of the cortical surface. Morphologies of 15 recorded layer 4 cells were successfully reconstructed (see Fig. 1d and Supplementary Fig. 1), which confirmed that they were located in layer 4.

For recording in the dLGN, we made a square craniotomy of 1.5 mm × 1.5 mm approximately 2.5 mm posterior and 2 mm lateral to the bregma structure. We applied cell-attached recordings to collect spikes from single neurons. The spike signal was filtered at 10 kHz and sampled at 20 kHz. We recorded from dLGN relay neurons, characterized by robust visually evoked responses with low spontaneous activity, at a depth of 2500 – 3100 μm[51]. For recording in the TRN, we made a square craniotomy of 1.5 mm × 1.5 mm around 1.1 mm posterior and 1.6 mm lateral to the bregma structure, and carried out cell-attached recordings at a depth of 2400 – 3000 μm.

In vivo two-photon imaging guided recording

We tuned a mode-locked Ti:sapphire laser (MaiTai Broadband, Spectra-Physics, Mountain View, CA) at 890 nm with the output power at 60 – 300 mW for imaging fluorescently labeled neurons in layer 4, and adjusted the power according to the cell's fluorescence level. We filled the glass electrode, with ∼1 μm tip opening and 8 – 10 MΩ impedance, with ACSF containing 0.15 mM calcein (Invitrogen). We completely compensated the pipette capacitance. We navigated the pipette tip in the cortex and patched it onto a fluorescent soma as previously described[23]. After confirming a successful targeting, we released the positive pressure in the pipette (∼10 mbar) and applied a negative pressure (20 – 150 mbar) to form a loose seal (with 80 – 200 MΩ resistance). We directly determined the depth of the patched cell under the two-photon microscope. The depth of the recorded PV neurons

ranged from 365 – 455 μm below the pia. The recorded PV neurons all exhibited narrow spike waveforms, with an average through-to-peak interval of 0.32 ± 0.05 ms (n = 6).

Visual stimulation

We implemented the visual stimuli using Matlab with Psychophysics Toolbox and displayed them with a gamma-corrected LCD monitor (refresh rate 75 Hz, maximum luminance 280 cd/m^2) placed 0.25 m away from the right eye. We placed the center of the monitor at 45° Azimuth, 25° Elevation, and it covered ±35° horizontally and ±27° vertically of the mouse visual field. We made recordings in the monocular zone of the V1. We recorded spontaneous activity by applying a uniform grey background. To measure orientation tuning, we applied drifting single bars (4° × 60°, at a speed of 50°/s) of 12 directions (30° step) in a pseudorandom sequence. The visual stimulation with and without LED illumination were alternated, but the stimulus sequence was randomized independently for LED off and LED on trials. Therefore, data collection was randomized. We set the inter-stimulus interval at 10 s to allow a full recovery of ChR2 function from desensitization[52]. We applied five to ten sets of stimuli to each cell, with the sequence different between sets. For recordings in the dLGN and TRN, we applied both drifting bars and full-field drifting sinusoidal gratings (temporal frequency = 2 Hz, spatial frequency = 0.04 cycles/degree, 95% contrast) at 12 directions. We also mapped the receptive field with flash stimuli, either flash light squares (5° × 5°) or flash light bars (4° × 60°) of vertical orientation for 5 – 10 repetitions in a pseudorandom sequence.

Photostimulation

To photoactivate ChR2, we used a blue (470 nm) fiber-coupled LED (0.2 mm diameter, Doric Lenses) placed on top of the exposed cortical surface. LED light spanned the entire area of V1. We applied black pigment stained agar to prevent LED light from scattering and reaching the contralateral eye, and had verified that LED light did not directly stimulate the eye in wild-type mice. The LED was driven by the analog output from a NIDAQ board (National Instruments). The intensity of LED was around 5 mW (measured at the tip of the fiber).

Data analysis

We performed data analysis with custom-developed software (LabVIEW, National Instrument; and MATLAB, Mathworks), not blind to the conditions of the experiments. We counted the spikes evoked by drifting bars or drifting sinusoidal gratings within a time window covering the visual stimulation duration with a 70 ms delay, and subtracted the spontaneous firing rate from the stimulus-evoked spike rate. We averaged the recorded synaptic responses, and smoothed it by averaging within a sliding 40 ms window[53].

We quantified the strength of orientation selectivity with a global orientation selectivity index (gOSI):

$$gOSI = \| \sum R(\theta) \times e^{2i\theta} \| / \sum R(\theta)$$

i is $\sqrt{-1}$ θ is the angle of the moving direction. $R(\theta)$ is the response level at angle θ. We averaged the response levels of two directions at the same orientation to obtain the orientation tuning curve between 0 – 180 degrees, and fitted it with a Gaussian function $R(\theta) = A \times \exp(-0.5 \times (\theta - \varphi)^2 / \sigma^2) + B$. φ is the preferred orientation. σ is the tuning width. To measure the direction selectivity index (DSI), we fitted the response levels at twelve stimulus directions to a wrapped Gaussian function $R(\theta) = A_1 \times \exp(-0.5 \times (\theta - \varphi)^2 / \sigma^2) + A_2 \times \exp(-0.5 \times (\theta - \varphi - 180°)^2 / \sigma^2) + B$. φ is the preferred direction. σ is the tuning width. DSI was defined as $(A_1 - A_2) / (A_1 + A_2 + 2B)$.

LED illumination alone led to a decrease in input resistance (from 181 ± 22 to 118 ± 24 MΩ, $P = 0.002$, one-tailed paired t-test, $n = 5$ cells from 5 mice), which was measured by examining the voltage change to a 100 pA step current. We estimated how much the decrease of input resistance would affect the recorded current amplitude based on the following equation[15]:

$$I_{rec} = \frac{R_{in}}{R_{in} + R_s} \times I_{syn}$$

I_{syn} is the actual amplitude of synaptic current. I_{rec} is the recorded amplitude. R_{in} is the input resistance. R_s is the effective series resistance (15∼30 MΩ) in our recordings, which was unchanged after cortical silencing). The decrease of R_{in} from 181 to 118 MΩ would lead to a 4% ∼ 7% reduction of the recorded synaptic amplitude, which is negligible compared to the measured amplitude reduction after cortical silencing (Fig. 2f). It should be noted that the putative change in recorded current amplitudes due to the change in input resistance would not significantly affect the tuning of synaptic responses. Similarly as we have previously discussed[15,40,54], under our recording condition, the observed synaptic responses can be reasonably controlled by the somatic voltage clamp. This was suggested by the linear $I - V$ relationship and the proximity of LED-evoked currents to the expected reversal potential of inhibitory currents (Fig. 1d). The thalamocortical synapses on layer 4 neurons have been shown to be proximal to the soma[55]. These synaptic inputs would be less affected by changes in input resistance compared to inputs onto distal dendrites[56]. Nevertheless, potential deviations of measured synaptic amplitudes from bona fide amplitudes caused by space-clamp errors and cable attenuation should be recognized[57–59].

To derive receptive field boundaries, we translated the onset delay of each drifting-bar response (after compensation for the subcortical conduction delay as determined from the cell's response to flash noise stimuli, see Fig. 4b) into the distance the bar had moved. To determine the response onset, we first identified the time point where the peak current occurred, and then traced current backward from the peak time to the time point where the amplitude was reduced to 5% of the peak value. We also visually examined response traces to confirm the determined onsets. The lines marking the bar positions at the compensated response onsets intercepted to form a dodecagon that outlined the spatial receptive field. We determined the midpoint of each side of the dodecagon, and performed the least squares fitting to an ellipse for the twelve midpoints. We defined the receptive field size as the

length of the major axis of the ellipse, and the aspect ratio as the ratio of the major versus minor axis of the ellipse.

For flash stimuli, we identified the visually evoked responses if the average peak current was 3 standard deviations greater than the baseline current in the absence of visual stimuli. For synaptic responses to flash squares, we fitted the receptive field to an elliptic function, and determined the receptive field boundary as previously described[29].

Statistical analysis

We first performed Shapiro–Wilk test to test whether data were normally distributed. In the case of a normal distribution, we performed paired *t*-test. Otherwise, we performed non-parametric method (Wilcoxon signed-rank test in this study). In fact, non-parametric and parametric methods led to the same conclusions. For multiple comparisons of normally distributed data, we applied one-way ANOVA followed by appropriate post-hoc tests, which was selected based on the test of homogeneity of variances. Data were presented as mean ± s.d. if not otherwise specified. No statistical method was used to pre-determine sample sizes, but our sample sizes were similar to those reported in previous publications in the field[8,16,37,41]

Supplementary Material

Refer to Web version on PubMed Central for supplementary material.

Acknowledgement

This work was supported by grants to H.W.T. from the US National Institutes of Health (EY019049 and EY022478) and the Kirchgessner Foundation. H.W.T. conceived and designed the study. Y.L., and L.I.A. performed the experiment. Y.L. and L.I.Z. performed data analysis. B.L. contributed data on direction tuning. H.W.T. wrote the paper. We thank Dr. M. Scanziani for the help on viral injection setup.

Reference

1. Douglas RJ, Martin KA. A functional microcircuit for cat visual cortex. J Physiol. 1991; 440:735–769. [PubMed: 1666655]
2. Callaway EM. Local circuits in primary visual cortex of the macaque monkey. Annu Rev Neurosci. 1998; 21:47–74. [PubMed: 9530491]
3. Hubel DH, Wiesel TN. Receptive fields, binocular interaction and functional architecture in the cat's visual cortex. J Physiol. 1962; 160:106–154. [PubMed: 14449617]
4. Reid RC, Alonso JM. Specificity of monosynaptic connections from thalamus to visual cortex. Nature. 1995; 378:281–284. [PubMed: 7477347]
5. Lampl I, Anderson JS, Gillespie DC, Ferster D. Prediction of orientation selectivity from receptive field architecture in simple cells of cat visual cortex. Neuron. 2001; 30:263–274. [PubMed: 11343660]
6. Ferster D, Miller KD. Neural mechanisms of orientation selectivity in the visual cortex. Annu Rev Neurosci. 2000; 23:441–471. [PubMed: 10845071]
7. Ferster D, Chung S, Wheat H. Orientation selectivity of thalamic input to simple cells of cat visual cortex. Nature. 1996; 380:249–252. [PubMed: 8637573]
8. Chung S, Ferster D. Strength and orientation tuning of the thalamic input to simple cells revealed by electrically evoked cortical suppression. Neuron. 1998; 20:1177–1189. [PubMed: 9655505]

9. Ben-Yishai R, Bar-Or RL, Sompolinsky H. Theory of orientation tuning in visual cortex. Proc Natl Acad Sci U S A. 1995; 92:3844–3848. [PubMed: 7731993]
10. Somers DC, Nelson SB, Sur M. An emergent model of orientation selectivity in cat visual cortical simple cells. J Neurosci. 1995; 15:5448–5465. [PubMed: 7643194]
11. Douglas RJ, Koch C, Mahowald M, Martin KA, Suarez HH. Recurrent excitation in neocortical circuits. Science. 1995; 269:981–985. [PubMed: 7638624]
12. Ben-Yishai R, Hansel D, Sompolinsky H. Traveling waves and the processing of weakly tuned inputs in a cortical network module. J Comput Neurosci. 1997; 4:57–77. [PubMed: 9046452]
13. Adorjan P, Levitt JB, Lund JS, Obermayer K. A model for the intracortical origin of orientation preference and tuning in macaque striate cortex. Vis Neurosci. 1999; 16:303–318. [PubMed: 10367965]
14. McLaughlin D, Shapley R, Shelley M, Wielaard DJ. A neuronal network model of macaque primary visual cortex (V1): orientation selectivity and dynamics in the input layer 4Calpha. Proc Natl Acad Sci U S A. 2000; 97:8087–8092. [PubMed: 10869422]
15. Liu BH, Wu GK, Arbuckle R, Tao HW, Zhang LI. Defining cortical frequency tuning with recurrent excitatory circuitry. Nat Neurosci. 2007; 10:1594–1600. [PubMed: 17994013]
16. Khibnik LA, Cho KK, Bear MF. Relative contribution of feedforward excitatory connections to expression of ocular dominance plasticity in layer 4 of visual cortex. Neuron. 2010; 66:493–500. [PubMed: 20510854]
17. Yamauchi T, Hori T, Takahashi T. Presynaptic inhibition by muscimol through GABAB receptors. European Journal of Neuroscience. 2000; 12:3433–3436. [PubMed: 10998126]
18. Porter JT, Nieves D. Presynaptic GABAB receptors modulate thalamic excitation of inhibitory and excitatory neurons in the mouse barrel cortex. J Neurophysiol. 2004; 92:2762–2770. [PubMed: 15254073]
19. Zhang F, Aravanis AM, Adamantidis A, de Lecea L, Deisseroth K. Circuit-breakers: optical technologies for probing neural signals and systems. Nat Rev Neurosci. 2007; 8:577–581. [PubMed: 17643087]
20. Bernstein JG, Garrity PA, Boyden ES. Optogenetics and thermogenetics: technologies for controlling the activity of targeted cells within intact neural circuits. Current opinion in neurobiology. 2012; 22:61–71. [PubMed: 22119320]
21. Olsen SR, Bortone DS, Adesnik H, Scanziani M. Gain control by layer six in cortical circuits of vision. Nature. 2012
22. Ma WP, et al. Visual representations by cortical somatostatin inhibitory neurons--selective but with weak and delayed responses. J Neurosci. 2010; 30:14371–14379. [PubMed: 20980594]
23. Liu BH, et al. Visual receptive field structure of cortical inhibitory neurons revealed by two-photon imaging guided recording. J Neurosci. 2009; 29:10520–10532. [PubMed: 19710305]
24. Katzner S, et al. Local Origin of Field Potentials in Visual Cortex. Neuron. 2009; 61:35–41. [PubMed: 19146811]
25. Pfrieger FW, Gottmann K, Lux HD. Kinetics of GABAB receptor-mediated inhibition of calcium currents and excitatory synaptic transmission in hippocampal neurons in vitro. Neuron. 1994; 12:97–107. [PubMed: 8292363]
26. Niell CM, Stryker MP. Highly selective receptive fields in mouse visual cortex. J Neurosci. 2008; 28:7520–7536. [PubMed: 18650330]
27. Priebe NJ, Ferster D. Inhibition, spike threshold, and stimulus selectivity in primary visual cortex. Neuron. 2008; 57:482–497. [PubMed: 18304479]
28. Volgushev M, Vidyasagar TR, Pei X. A linear model fails to predict orientation selectivity of cells in the cat visual cortex. J Physiol. 1996; 496(Pt 3):597–606. [PubMed: 8930828]
29. Cruikshank SJ, Urabe H, Nurmikko AV, Connors BW. Pathway-specific feedforward circuits between thalamus and neocortex revealed by selective optical stimulation of axons. Neuron. 2010; 65:230–245. [PubMed: 20152129]
30. Piscopo DM, El-Danaf RN, Huberman AD, Niell CM. Diverse visual features encoded in mouse lateral geniculate nucleus. J Neurosci. 2013; 33:4642–4656. [PubMed: 23486939]

31. Bruno RM, Sakmann B. Cortex is driven by weak but synchronously active thalamocortical synapses. Science. 2006; 312:1622–1627. [PubMed: 16778049]
32. Jin J, Wang Y, Swadlow HA, Alonso JM. Population receptive fields of ON and OFF thalamic inputs to an orientation column in visual cortex. Nat Neurosci. 2011; 14:232–238. [PubMed: 21217765]
33. Kerlin AM, Andermann ML, Berezovskii VK, Reid RC. Broadly tuned response properties of diverse inhibitory neuron subtypes in mouse visual cortex. Neuron. 2010; 67:858–871. [PubMed: 20826316]
34. Ko H, et al. Functional specificity of local synaptic connections in neocortical networks. Nature. 2011
35. Liu BH, et al. Broad inhibition sharpens orientation selectivity by expanding input dynamic range in mouse simple cells. Neuron. 2011; 71:542–554. [PubMed: 21835349]
36. Li YT, et al. Broadening of Inhibitory Tuning Underlies Contrast-Dependent Sharpening of Orientation Selectivity in Mouse Visual Cortex. J Neurosci. 2012; 32:16466–16477. [PubMed: 23152629]
37. Atallah BV, Bruns W, Carandini M, Scanziani M. Parvalbumin-expressing interneurons linearly transform cortical responses to visual stimuli. Neuron. 2012; 73:159–170. [PubMed: 22243754]
38. Wilson NR, Runyan CA, Wang FL, Sur M. Division and subtraction by distinct cortical inhibitory networks in vivo. Nature. 2012; 488:343–348. [PubMed: 22878717]
39. Lee SH, et al. Activation of specific interneurons improves V1 feature selectivity and visual perception. Nature. 2012; 488:379–383. [PubMed: 22878719]
40. Liu BH, et al. Intervening inhibition underlies simple-cell receptive field structure in visual cortex. Nat Neurosci. 2010; 13:89–96. [PubMed: 19946318]
41. Tan AY, Brown BD, Scholl B, Mohanty D, Priebe NJ. Orientation selectivity of synaptic input to neurons in mouse and cat primary visual cortex. J Neurosci. 2011; 31:12339–12350. [PubMed: 21865476]
42. Katzner S, Busse L, Carandini M. GABAA inhibition controls response gain in visual cortex. J Neurosci. 2011; 31:5931–5941. [PubMed: 21508218]
43. Branco T, Clark BA, Hausser M. Dendritic discrimination of temporal input sequences in cortical neurons. Science. 2010; 329:1671–1675. [PubMed: 20705816]
44. Ohki K, Chung S, Ch'ng YH, Kara P, Reid RC. Functional imaging with cellular resolution reveals precise micro-architecture in visual cortex. Nature. 2005; 433:597–603. [PubMed: 15660108]
45. Allman J, Miezin F, McGuinness E. Stimulus specific responses from beyond the classical receptive field: neurophysiological mechanisms for local-global comparisons in visual neurons. Annual review of neuroscience. 1985; 8:407–430.
46. Gilbert CD, Wiesel TN. The influence of contextual stimuli on the orientation selectivity of cells in primary visual cortex of the cat. Vision Res. 1990; 30:1689–1701. [PubMed: 2288084]
47. Levitt JB, Lund JS. Contrast dependence of contextual effects in primate visual cortex. Nature. 1997; 387:73–76. [PubMed: 9139823]
48. Chisum HJ, Mooser F, Fitzpatrick D. Emergent properties of layer 2/3 neurons reflect the collinear arrangement of horizontal connections in tree shrew visual cortex. J Neurosci. 2003; 23:2947–2960. [PubMed: 12684482]
49. Clopath C, Busing L, Vasilaki E, Gerstner W. Connectivity reflects coding: a model of voltage-based STDP with homeostasis. Nat Neurosci. 2010; 13:344–352. [PubMed: 20098420]
50. Ko H, et al. The emergence of functional microcircuits in visual cortex. Nature. 2013; 496:96–100. [PubMed: 23552948]
51. Grubb MS, Thompson ID. Quantitative characterization of visual response properties in the mouse dorsal lateral geniculate nucleus. J Neurophysiol. 2003; 90:3594–3607. [PubMed: 12944530]
52. Lin JY, Lin MZ, Steinbach P, Tsien RY. Characterization of engineered channelrhodopsin variants with improved properties and kinetics. Biophys J. 2009; 96:1803–1814. [PubMed: 19254539]
53. Li YT, Ma WP, Pan CJ, Zhang LI, Tao HW. Broadening of Cortical Inhibition Mediates Developmental Sharpening of Orientation Selectivity. The Journal of Neuroscience. 2012; 32:3981–3991. [PubMed: 22442065]

54. Wu GK, Li P, Tao HW, Zhang LI. Nonmonotonic synaptic excitation and imbalanced inhibition underlying cortical intensity tuning. Neuron. 2006; 52:705–715. [PubMed: 17114053]

55. Petreanu L, Mao T, Sternson SM, Svoboda K. The subcellular organization of neocortical excitatory connections. Nature. 2009; 457:1142–1145. [PubMed: 19151697]

56. Zhang M, et al. Functional elimination of excitatory feedforward inputs underlies developmental refinement of visual receptive fields in zebrafish. J Neurosci. 2011; 31:5460–5469. [PubMed: 21471382]

57. Wehr M, Zador AM. Balanced inhibition underlies tuning and sharpens spike timing in auditory cortex. Nature. 2003; 426:442–446. [PubMed: 14647382]

58. Wu GK, Tao HW, Zhang LI. From elementary synaptic circuits to information processing in primary auditory cortex. Neurosci Biobehav Rev. 2011; 35:2094–2104. [PubMed: 21609731]

59. Tan AY, Zhang LI, Merzenich MM, Schreiner CE. Tone-evoked excitatory and inhibitory synaptic conductances of primary auditory cortex neurons. J Neurophysiol. 2004; 92:630–643. [PubMed: 14999047]

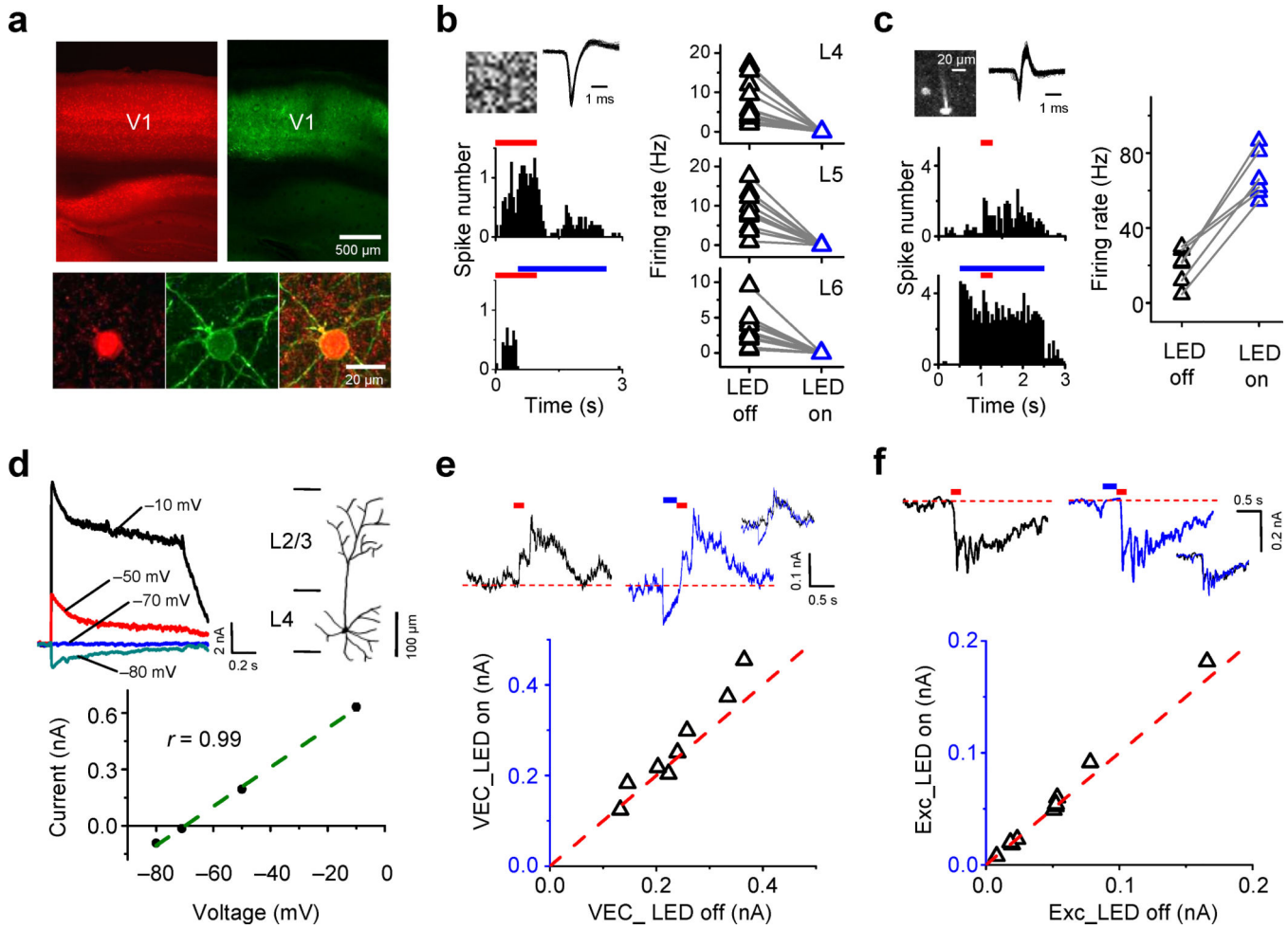

Figure 1.

Optogenetic silencing of visual cortical circuits. (**a**) Top, confocal images showing tdTomato (red) and ChR2-EYFP expression (green) patterns. Bottom, enlarged images. (**b**) Left, peri-stimulus spike time histograms (PSTHs) for responses of a layer 4 excitatory neuron to a flash noise stimulus (red bar) with and without LED illumination (blue bar). Top, visual stimulus pattern and superimposed 50 individual spikes. Right, average firing rates in LED off and LED on trials for cells in different layers (n = 14, 10, 11 from 6, 5, 5 mice for L4, L5, L6 respectively). (**c**) Left, PSTHs for responses of a tdTomato-labeled PV neuron. Top inset, two-photon image of the recorded cell and superimposed 100 individual spikes. Right, Average firing rates for 6 PV cells from 6 mice. (**d**) Top, LED illumination induced currents in a cell and its reconstructed morphology. Bottom, current amplitude (averaged within a 40 ms window) versus holding voltage (one-sided P = 0.005). (**e**) Top, visually-evoked ensemble currents (VEC) recorded in layer 4 without (left) and with (right) preceding LED illumination. Inset, superimposed traces. Bottom, peak amplitudes in LED on versus LED off trials (0.26 ± 0.11 vs. 0.24 ± 0.08 nA, P = 0.07, two-tailed paired t-test, n = 8 sites from 8 mice). (**f**) Top, visually-evoked excitatory currents without and with a preceding LED illumination. Bottom, peak amplitudes in LED on versus LED off trials

(median: 0.051 vs. 0.051 nA, $P = 0.23$, two-sided Wilcoxon signed-rank test, $n = 10$ cells from 10 mice).

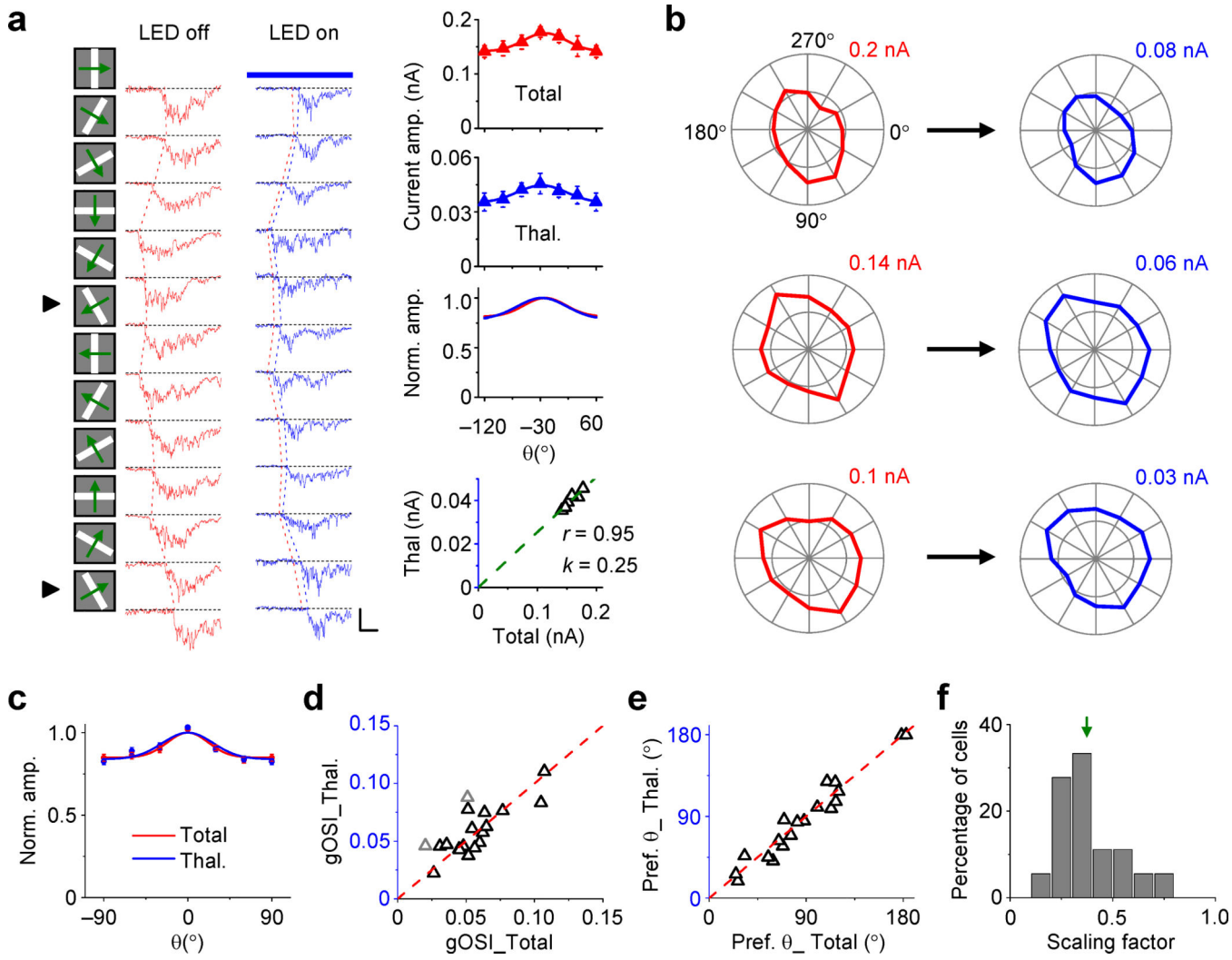

Figure 2.

Linear amplification of orientation-tuned thalamocortical input. (**a**) Left, average excitatory responses (5 trails) of a cell to single drifting bars at 12 different directions. Arrowheads mark the preferred orientation. Light red and light blue dotted curves mark the response onsets. Scale: 0.1 (red)/ 0.04 (blue) nA, 0.5 s. Right top, orientation tuning curves of peak current amplitude for the total and thalamocortical excitation, as well as superimposed normalized tuning curves. Bar = s.d. Right bottom, peak current amplitudes at 6 orientations of LED on versus LED off trials. Dash line shows the linear fitting: "*k*" is the slope, "*r*" is the correlation coefficient, one-sided $P = 0.0009$. (**b**) Polar plots of excitatory current amplitude before (red) and after (blue) silencing the cortex for another three cells. The maximum axis value is labeled. (**c**) Average normalized orientation tuning curves of total excitatory input (red) and of thalamocortical input (blue). Bar = s.e.m. $N = 19$ cells from 19 mice. (**d**) OSI of thalamocortical input versus that of total excitation (0.059 ± 0.021 vs. 0.056 ± 0.023, $P = 0.4$, two-tailed paired *t*-test, $n = 19$ cells). Light gray labels individual cells that deviate significantly from the identity line ($P < 0.05$, bootstrap analysis). (**e**) Preferred orientation of thalamocortical input versus that of total excitation ($P = 0.6$, two-

tailed paired *t*-test, $n = 19$ cells). (**f**) Distribution of scaling factors in the recorded cell population. Arrow points to the mean value.

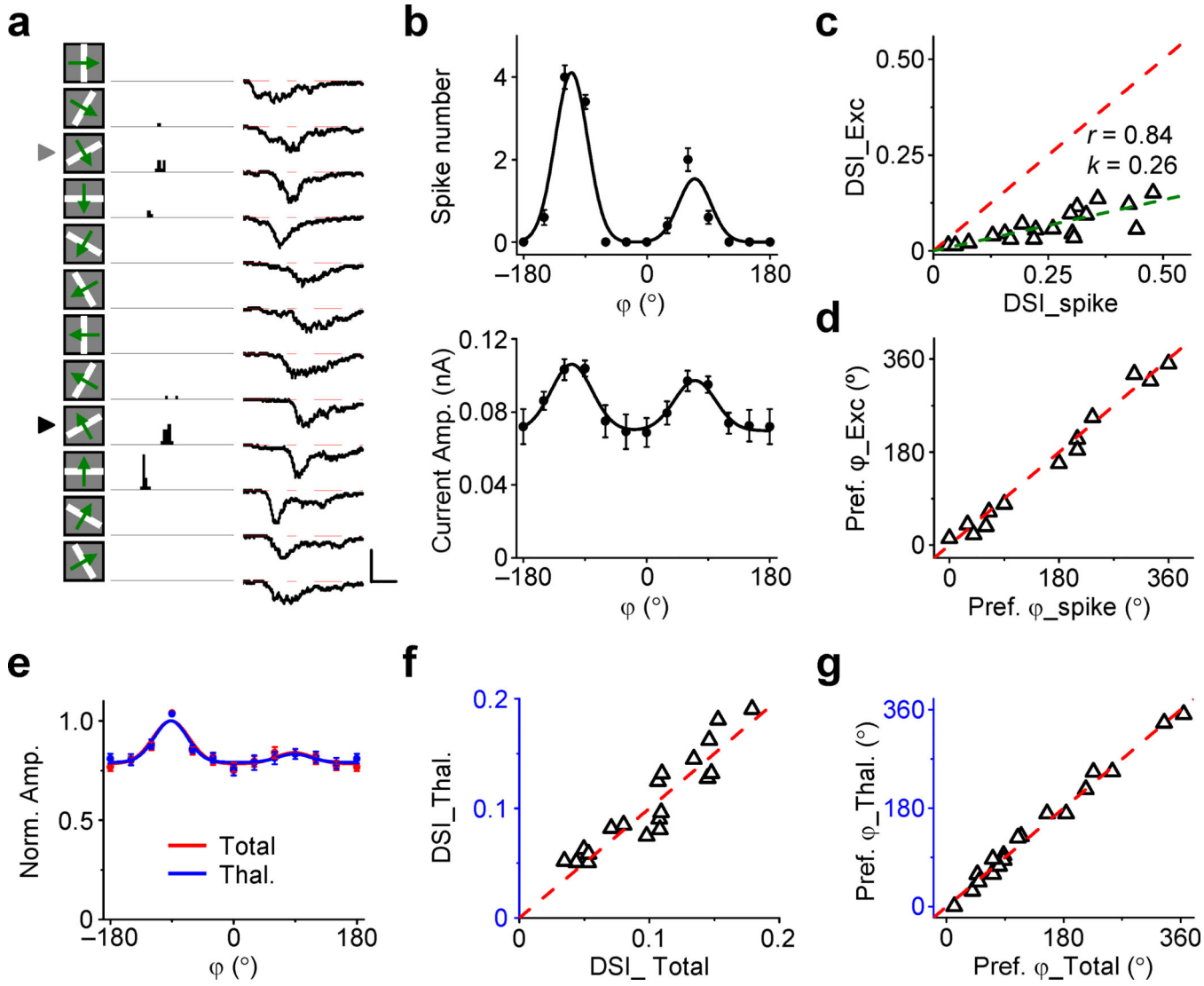

Figure 3.

Intracortical excitation preserves direction tuning. (**a**) PSTH for spike responses (left, 10 trials) to single drifting bars of an example layer 4 cell as well as its average excitatory responses (right, 10 trials) recorded under voltage clamp. Scale: 30 Hz / 0.1 nA, 0.5 s. (**b**) Top, tuning curve of average spike count (10 trials) for the same cell. Bottom, tuning curve of average peak excitatory current. Bar = s.d. (**c**) Direction selectivity index (DSI) of excitatory input versus that of spike response (n = 20 cells from 20 mice). Linear fitting (olive dash line): one-sided P = 1e–5. (**d**) Preferred direction of excitatory input versus that of spike response for cells with DSI > 0.2 (P = 0.3, two-tailed paired t-test, n = 13 cells from 13 mice). (**e**) Average normalized direction tuning curves for total excitation (red) and thalamocortical excitation (blue). Bar = s.e.m. N = 19 cells from 19 mice. (**f**) DSI for thalamocortical excitation versus that for total excitation (0.104 ± 0.045 vs. 0.102 ± 0.043, P = 0.49, two-tailed paired t-test, n = 19 cells from 19 mice). (**g**) Preferred direction of thalamocortical excitation versus that of total excitation (P = 0.86, two-tailed paired t-test, n = 19 cells).

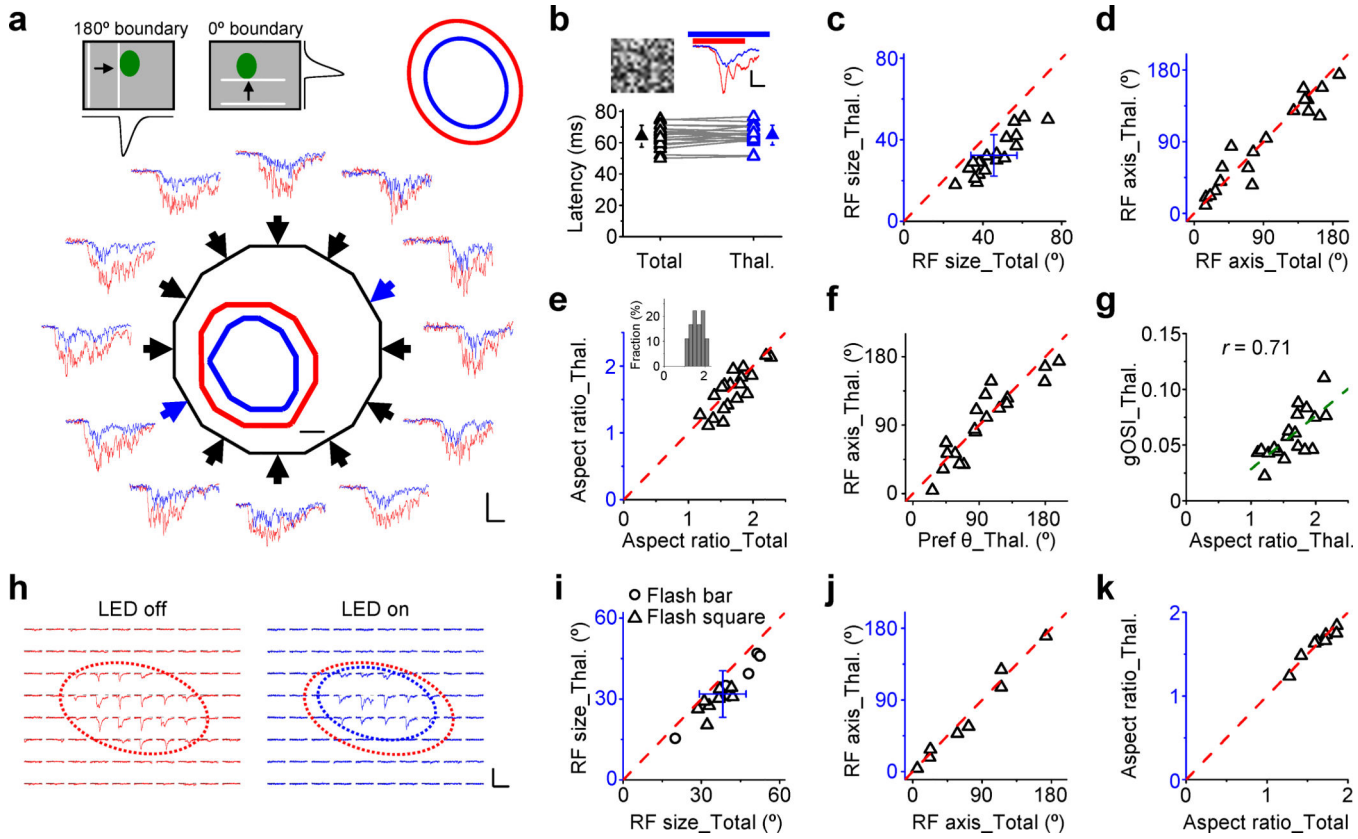

Figure 4.

Intracortical excitation expands visual receptive field. (**a**) Top left, stimulation of receptive field (green) boundary correlates with the response delay. Bottom, superimposed average bar-evoked excitatory currents without (red) and with (blue) LED illumination. Scale: 0.1 nA (red)/ 0.05 nA (blue), 0.5 s. Inside dodecagon: derived receptive fields before (red) and after (blue) cortical silencing. Scale: 10°. Top right, elliptical fitting of the receptive fields. (**b**) Top, average excitatory currents to a flash noise stimulus. Scale: 50 pA, 50 ms. Bottom, onset latencies in LED off versus LED on trials (64.1 ± 6.9 vs. 64.8 ± 6.3 ms, $P = 0.32$, two-tailed paired *t*-test, $n = 19$ cells from 19 mice; the same test applied below). Error bars represent s.d. (**c**) Receptive field size derived for thalamocortical and total excitation (mean ± s.d. marked). (**d**) Angle of receptive field major axis ($P = 0.52$). (**e**) Aspect ratio (1.63 ± 0.32 vs. 1.68 ± 0.29). Inset, distribution of aspect ratios of thalamocortical receptive fields. (**f**) Derived major receptive field axis versus measured preferred orientation ($P = 0.54$). (**g**) OSI versus aspect ratio. Linear fitting: one-sided $P = 3.3e{-}4$. (**h**) Excitatory currents of an example cell to single flash squares at different locations without and with LED stimulation. Scale: 0.1 nA (left) / 0.052 nA (right), 0.2 s. (**i-k**) Receptive fields measured by flash stimuli ($n = 14$ cells from 14 mice). $P = 0.4$ in (**j**). Aspect ratios in (**k**): 1.60 ± 0.21 vs. 1.58 ± 0.21, $P = 0.46$.

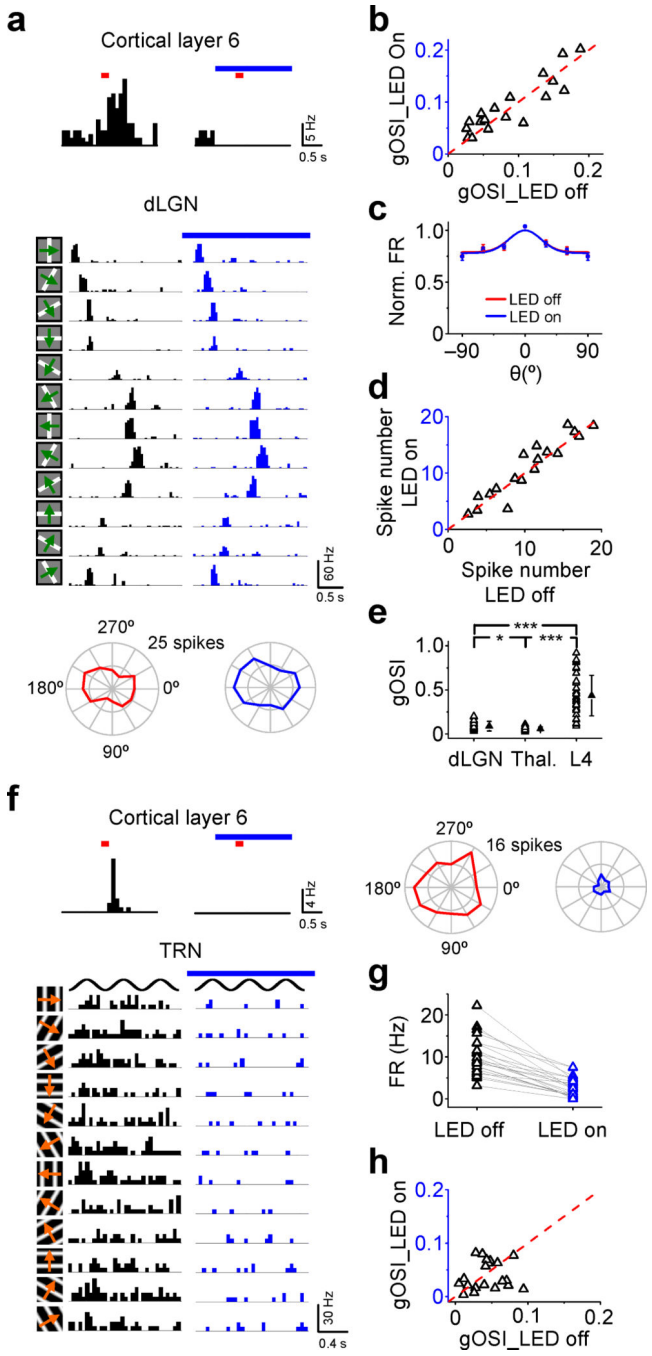

Figure 5.

Orientation tuning of thalamic neurons. (**a**) Top, PSTHs for visually evoked spikes in a layer 6 neuron. Middle, PSTHs for responses to drifting bars without (black) and with (blue) LED illumination of a dLGN neuron in the same animal. Bottom, polar plots of average spike count. (**b**) OSI of dLGN neuron responses (LED on, 0.093 ± 0.052; LED off, 0.089 ± 0.054, $P = 0.48$, two-tailed paired *t*-test, $n = 18$ cells from 12 mice). (**c**) Average normalized tuning curves for dLGN neurons. Bar = s.e.m. (**d**) Evoked spike numbers for dLGN neurons (LED on, 10.4 ± 4.9; LED off, 10.9 ± 5.3; $P = 0.27$, two-tailed paired *t*-test, $n = 18$ cells from 12

mice). (**e**) Distribution of OSIs for dLGN neuron spikes, thalamocortical excitation, and layer 4 neuron spikes to drifting bars (n = 18, 19, 33 cells from 12, 19, 25 mice respectively). ***, P = 5.4e–10 and 1.4e–11 (top); *, P = 0.022, one-way ANOVA post-hoc test (Tamhane's T2 test). Error bars represent s.d. (**f**) Spike responses of an example TRN neuron to drifting gratings (three cycles). Data are displayed similarly as in (**a**). (**g**) Average evoked firing rates of TRN neurons (LED on, 2.8 ± 2.3; LED off, 10.2 ± 4.6 Hz, P = 3.6e–9, one-tailed paired t-test, n = 20 cells from 16 mice). (**h**) OSI of TRN neuron responses (LED on, 0.040 ± 0.027; LED off, 0.044 ± 0.025, P = 0.59, two-tailed paired t-test, n = 20 cells from 16 mice).